Doping and thickness dependent electrical characteristics of backgated silicon nanowire biosensors

By

Md. Asrarul Haque

(ID: 2011-1-80-025)

And

Kaishar Uddin

(ID: 2011-1-80-068)

And

Md. Rouzatun Rafiue

(ID: 2011-1-80-060)

Submitted to the

Department of Electrical & Electronics Engineering, Faculty of Science and Engineering

East West University

In fulfillment of the requirements for the degree of Bachelor of Science in Electrical & Electronics Engineering

(B.Sc. in EEE)

Summer, 2015

Approved By

Academic Advisor	Department Chairperson
Dr. Mohammad Mojammel Al Hakim	Dr. Halima Begum

Approval

The thesis title "Tuning Si NW electrical characteristics through backgate bias arrangement and feasibility of its application as a biosensor" submitted by Md. Asrarul Haque [2011-1-80-025], Kaishar Uddin [2011-1-80-068] and Md. Rouzatun Rafiue [2011-1-80-060] in the semester of summer, 2015 is approved satisfactory in fulfilling the requirements for the degree of Bachelor of Science in Electrical and Electronics Engineering.

Dr. Mohammad Mojammel Al Hakim

Associate Professor, Department of Electrical and Electronics Engineering

East West University, Dhaka, Bangladesh

Declaration

We, hereby certify that our thesis work solely to be our own scholarly work. To the best of our knowledge, it has not been collected from any source without the due acknowledgement and permission. It is being submitted in fulfilling the requirements for the degree of Bachelor of Science in Electrical and Electronics Engineering. It has been submitted before any degree or examination of any other university.

_____

Md. Asrarul Haque

_____

Kaishar Uddin

_____

Md. Rouzatun Rafiue

Summer Semester

August 2015

Abstract

We performed a feasibility study of Si nanowire as a biosensor through backgate bias arrangement by tuning its electrical characteristics. 75nm, 50nm and 25nm thick Si NW having channel length of 1µm with doping concentrations of $10^{16}cm^{-3}$, $10^{17}cm^{-3}$ and $10^{18}cm^{-3}$ respectively were investigated for different backgate voltages. It is found that backgate bias has a significant effect on the sensitivity of p-type Si-NW. 75nm thick NW shows sub-threshold slope of 70.36mV/dec, 79mV/dec and 3402.2mV/dec at doping values of $10^{16}cm^{-3}$, $10^{17}cm^{-3}$ and 10^{18} cm^{-3} respectively. This result shows that 75nm thick Si NW's sensor characteristics degrade with the increase of body doping values. Application of positive backgate has been found to improve NW's sub-threshold characteristics however this improvement is minor for 75 nm thick Si NW at $10^{18}cm^{-3}$ doping. The 25nm thick Si NW exhibited sub-threshold slopes of 64mV/dec, 65.49mV/dec and 66.96mV/dec at doping values of $10^{16}cm^{-3}$, $10^{17}cm^{-3}$ and $10^{18}cm^{-3}$ respectively which implies much better sensor operation of 25nm thick NW in comparison to 75 nm thick NW. Application of +7V of positive backgate bias resulted in the improvement of the sub-threshold slope of the 25nm thick NW with values of 62mV/dec, 62mV/dec and 63.11mV/dec at doping values of $10^{16}cm^{-3}$, $10^{17}cm^{-3}$ and $10^{18}cm^{-3}$ respectively. In all cases application of negative backgate bias generally degrades the sub-threshold behavior of NW's. These results show that backgate bias arrangement has significant effect on NW sensor operation. A typical less sensitive NW can be converted into a sensitive one by choosing the appropriate backgate voltage. However this thesis also gives a data base of NW thickness and doping for sensor design. These results are very important for p-type Si-NW based biosensors fabricated on SOI platform to ensure maximum sensitive operation for molecular level detection.

Acknowledgment

It is with enormous appreciation that we acknowledge the contribution of our supervisor, Dr. Mohammad Mojammel Al Hakim, Associate Professor of Department of Electrical and Electronics Engineering, East West University. Without his proper guidance, encouragement and support this thesis would have remained a dream. We consider it as an honor to work with him. We are also indebted to our parents, other professors of the department and friends for their support and encouragements. Finally thanks to Almighty who gave us the patience to complete the task successfully.

Authorization Page

We hereby certify that we are the sole authors of this thesis. We authorize East West University to lend this thesis to other institutions or individuals for the purpose of scholarly research only after one year of the submission.

_____

Md. Asrarul Haque

_____

Kaishar Uddin

_____

Md. Rouzatun Rafiue

We authorize East West University to produce this thesis by photocopy or other means, in total or in part, at the request of other institutions or individuals for the purpose of scholarly research only after one year of the submission.

_____

_____

_____

Table of Contents

Page number

List of Figures

Page number

List of Tables

Page number

CHAPTER 1: INTRODUCTION

1.1 Background, Motivation and Objective

A silicon nanowire field effect transistor (Si-NW-FET) replacing traditional FET's grabbed a lot of attention for their higher sensitivity and ability to detect any molecules or target materials instantly. [1-10] Nanowire or any nano-device comprises at least one dimension in nano range (10^{-9}) so they can provide this ultra sensitivity due to this very small size and large surface area to volume ratio. When target molecules bind to the surface of the nanowire a change in current is found due to field effect. The effect is so strong that the specific charge attached to the surface of the nanowire can deplete or accumulate the whole cross sectional area of the nanowire. Plenty of works could be found exploring Si NW as sensors.

Lieber et al. [3] successfully fabricated silicon nanowire biosensors on p-type semiconductor where linear characteristics were found for the typical DC current voltage (I-V). The capability of the fabricated nano-biosensors was tested for pH response with or without modifying nanowire surface containing both amino or silanol receptor. It was shown that increment of the pH level of the solution resulted in the increase of conductance of Si nanowire due to the increment of hydroxyl ions (negatively charged ions) in the solution and vice versa with typical sensitivity around 10% to 20% only. Instant detection of clinically relevant protein streptavidin was confirmed down to even extremely lower concentrations such of 10pM (pico molar). Single DNA and wild type virus (DF508) could also be detected. This electrical detection was found down to concentration of 60fM (femto molar). These nanowires show promise as sensitive biosensors and intrinsic DC characteristics were linear so it behaves like a simple constricted dimension resistors.

Chen et al. [11] fabricated p-type silicon nanowires using a new size reduction method where silicon nanowires had a height of 140nm, width of 100nm with triangular structure and a uniform doping concentration of $N_a=10^{17}cm^{-3}$. The measured current-voltage (I-V) characteristics were non-linear like a diode. According to I-V curves that was provided, there were no conduction up to drain bias of $V_{ds}<1V$. The conduction of nanowires were improved through the application of negative backgate bias thereby increasing the accumulation of holes and at $V_{backgate} = -20V$, the I-V characteristics showed linear behavior. It is observable that at small negative $V_{backgate}$ the I-V characteristics are typically nonlinear. This was attributed to the fixed electronic charge located in the front oxide near the top silicon device layer surface and buried oxide near the bottom of silicon device layer due to reactive thermal oxidation of silicon surface. These nanowires also successfully sensed pH level of the solution with sensitivity around 40mV/pH.

Most recently, Jean-Pierre Colinge et al. [12] first time reported that Si nanowire with a few tens of nanometers wide, thickness of 20nm and uniform doping concentrations around $10^{19}cm^{-3}$, behaves like transistor than simple resistor. With the same principle both p-type and n-type silicon nanowires were fabricated and measured characteristics showed that both n-type and p-

type devices exhibited transistor action. These devices gave sub-threshold slope of 64mV/ decade with quite good output characteristics.

The aforementioned analysis shows quite variable DC characteristics that have been reported for Si NW's. For sensitive operation NW's sub-threshold slope should be close to its theoretical best value of 60mV/dec which however may be dependent on NW thickness, doping and applied biases. So far there is no report available showing inherent thickness and doping dependency of sub-threshold characteristics of NW's and a study showing possibility of tuning behavior using backgate bias arrangement.

In this work we first time study the electrical characteristics of the Silicon nanowire for different backgate bias arrangement and for different NW thickness and doping concentration. Si-NWs are formed on SOI (Silicon on Insulator) wafers using top down approaches and its buried Si layer can be used as an additional gate to tune Si-NW's sensitivity. P-type Silicon nanowire thickness for 75nm, 50nm and 25nm with 1µm long (Channel length) with doping concentrations of $10^{16}/cm^3$, $10^{17}/cm^3$ and $10^{18}/cm^3$ have been investigated to find out the best combination for making immaculate bio-sensors.

1.2 Organization

Chapter 1 provides the necessary background for working on the electrical Characteristics of silicon nanowires. A number of research papers have been studied to get an understanding of NW sensors.

Chapter 2 describes device structure, simulation methodology and the required models for the simulation.

Chapter 3 describes the simulation results for nanowires having thicknesses of 75nm, 50nm and 25nm respectively with uniform doping concentrations of $10^{16}cm^{-3}$, $10^{17}cm^{-3}$ and $10^{18}cm^{-3}$ for different backgate bias conditions.

Finally, in chapter 4, the contribution of this work is summarized and discussed.

CHAPTER 2: METHODOLOGY

2.1 Device features and simulation models

The investigation on the sensitivity of Silicon nanowire for biosensor application were done with the help of numerical simulations using the software SILVACO Atlas device simulator [13], installed on the VLSI lab of East West University. A p-type silicon nanowire was created on 100nm oxide with a 500nm buried Si layer. A secondary gate (backgate) is made with 25nm Al beneath the buried Si layer. The gate oxide thickness was 2nm and a heavily doped poly-silicon layer was used as top gate material. In the silicon nanowire, two heavily doped regions on the two sides of the channel were employed to ensure ohmic contact on the source/drain regions. The gate doping was $10^{20}/cm^3$ and the source/drain regions were also heavily doped with the doping density of $10^{20}/cm^3$. Here, the gate doping was n-type whereas the drain and the channel doping was p-type. To contact source to drain and gate, aluminum electrode was chosen.

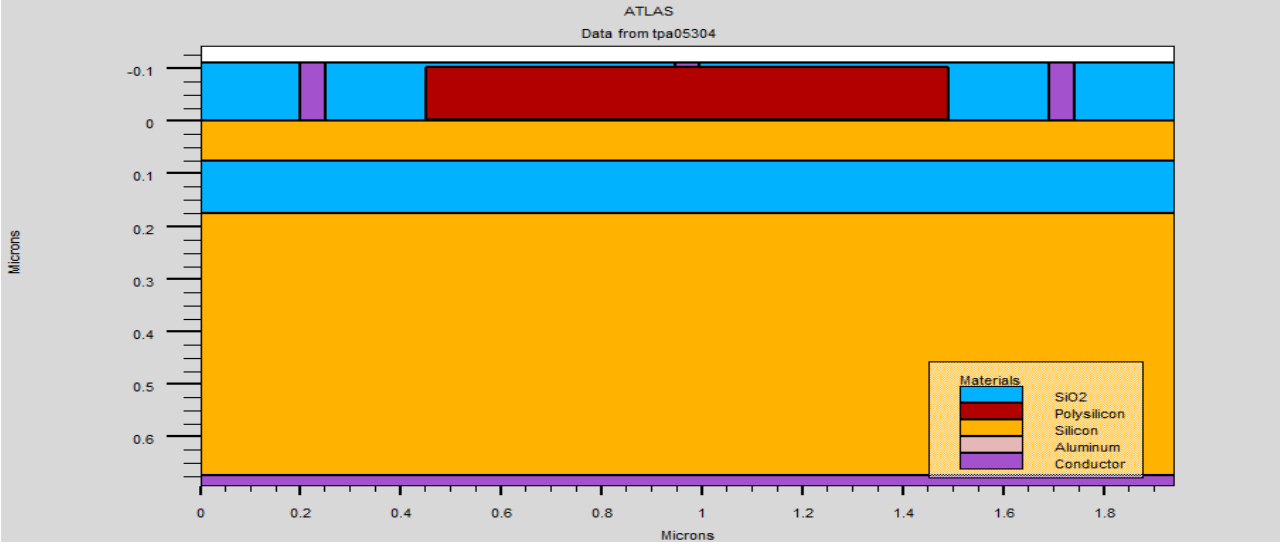

Figure 2.1: Schematic of the simulated p-type silicon nanowire.

In simulation our Si NW thicknesses were chosen at 75nm, 50nm and 25nm. Body doping of NW was also varied from $10^{16}/cm^3$ to $10^{18}/cm^3$ as Si-NW thickness 10nm quantum effect is neglected and a classical drift diffusion model is used to investigate Si-NW behavior. To accurately model carrier mobility in the constricted volume of NW Lombardi (CVT) model was used to take account temperature (T_L), perpendicular electric field ($E_\perp$), parallel electric field (E II) and doping concentration (N) effects [13]. In the CVT model, the transverse field, doping dependent and temperature dependent parts of the mobility are given by the three components that are combined using Mathiessen's rule. These components are surface mobility limited by scattering with acoustic photons (μ_{AC}), the mobility limited by surface roughness (μ_{SR}) and the mobility limited by scattering with optical intervalley photons (μ_b) are combined using Mathiessen's rule as follows[13]:

$$\mu_T^{-1} = \mu_{AC}^{-1} + \mu_b^{-1} + \mu_{sr}^{-1} \quad (2.1)$$

The first component, surface mobility limited by scattering with acoustic phonons equations [13]:

$$\mu_{AC.n} = \frac{BN.CVT}{E_\perp} + \frac{CN.CVT\ N^{\tau.CVT}}{T_L\ E_\perp^{1/3}} \quad (2.2)$$

$$\mu_{AC.p} = \frac{BN.CVT}{E_\perp} + \frac{CP.CVT\ N^{\tau P.CVT}}{T_L\ E_\perp^{1/3}} \quad (2.3)$$

The equation parameters BN.CVT, BP.CVT, CN.CVT, CP.CVT, TAUN.CVT, and TAUP.CVT used for this simulation are shown in Table 3-1 [13].

The second component, μ_{sr} is the surface roughness factor and is given by [13]:

$$\mu_{sr} = \frac{DELN.CVT}{E_\perp^2} \quad (2.4)$$

$$\mu_{sr} = \frac{DELP.CVT}{E_\perp^2} \quad (2.5)$$

The equation parameters DELN.CVT and DELP.CVT used for this simulation are shown in Table 3.1[13].

The third mobility component, the mobility limited by scattering with optical intervalley phonons is given by [13]:

$$\mu_{b,n} = MU0N.CVT exp\left(\frac{-PCN.CVT}{N}\right) + \frac{\left[MUMAXN.CVT\left(\frac{T_L}{300}\right)^{-GAMN.CVT} - MU0N.CVT\right]}{1+\left(\frac{N}{CRN.CVT}\right)^{ALPHN.CVT}} - \frac{MU1N.CVT}{1+\left(\frac{CSN.CVT}{N}\right)^{BETAN.CVT}} \quad (2.6)$$

$$\mu_{b,p} = MU0P.CVT exp\left(\frac{-PCP.CVT}{N}\right) + \frac{\left[MUMAXP.CVT\left(\frac{T_L}{300}\right)^{-GAMP.CVT} - MU0P.CVT\right]}{1+\left(\frac{N}{CRP.CVT}\right)^{ALPHP.CVT}} - \frac{MU1P.CVT}{1+\left(\frac{CSP.CVT}{N}\right)^{BETAP.CVT}} \quad (2.7)$$

Table 2.1: Parameters for Equations 2.1 to 2.7

Statement	Parameter	Default	Units
MOBILITY	BN.CVT	4.75×10^{7}	cm/(a)
MOBILITY	BP.CVT	9.925×10^{4}	cm/(a)
MOBILITY	CN.CVT	1.74×10^{5}	
MOBILITY	CP.CVT	8.842×10^{5}	
MOBILITY	TAUN.CVT	0.125	
MOBILITY	TAUP.CVT	0.0317	
MOBILITY	GAMN.CVT	2.5	
MOBILITY	GAMP.CVT	2.2	
MOBILITY	MU0N.CVT	52.2	$cm^2/(v\text{-}a)$
MOBILITY	MU0P.CVT	44.9	$cm^2/(v\text{-}a)$
MOBILITY	MU1N.CVT	43.4	$cm^2/(v\text{-}a)$
MOBILITY	MU1P.CVT	29.0	$cm^2/(v\text{-}a)$
MOBILITY	MUMAXN.CVT	1417.0	$cm^2/(v\text{-}a)$
MOBILITY	MUMAXP.CVT	470.5	$cm^2/(v\text{-}a)$
MOBILITY	CRN.CVT	9.68×10^{14}	cm^{-3}
MOBILITY	CRP.CVT	2.23×10^{17}	cm^{-3}
MOBILITY	CSN.CVT	3.43×10^{20}	cm^{-3}
MOBILITY	CSP.CVT	6.10×10^{20}	cm^{-3}
MOBILITY	ALPHN.CVT	0.680	
MOBILITY	ALPHP.CVT	0.71	
MOBILITY	BETAN.CVT	2.00	

MOBILITY	BETAP.CVT	2.00	
MOBILITY	PCN.CVT	0.0	cm^{-3}
MOBILITY	PCP.CVT	0.23×10^{16}	cm^{-3}
MOBILITY	DELN.CVT	5.82×10^{14}	v/s

The model for carrier emission and absorption processes proposed by Shockley-Read-Hall (SRH) is used to reflect the recombination phenomenon within the device. The electron and hole lifetimes $\tau_{n \text{ and }} \tau_p$ were modeled as concentration dependent. The equation is given by [13]:

$$R_{SRH} = \frac{pn - n_{ie}^2}{\tau_p\left[n + n_{ie}\exp\left(\frac{ETRAP}{kT_L}\right)\right] + \tau_n\left[p + n_{ie}exp\left(\frac{-ETRAP}{kT_L}\right)\right]} \quad (2.8)$$

$$\tau_n = \frac{TAUNO}{1 + \frac{N}{(NSRHN)}} \quad (2.9)$$

$$\tau_p = \frac{TAUPO}{1 + \frac{N}{(NSRHP)}} \quad (2.10)$$

Here N is called the local (total) impurity concentration. The used parameters TAUN0, TAUP0, NSRHN and NSRHP are Table 3-2[13]. This model was activated with the CONSRH parameter of the MODELS statement.

Table 2.2: Default Parameters for Equations 2.8 to 2.10

Statement	Parameter	Default	Units
METERIAL	TAUNO	1.0×10^{-7}	S
METERIAL	NSRHN	5.0×10^{16}	cm^{-3}
METERIAL	TAUPO	1.0×10^{-7}	S
METERIAL	NSRHP	5.0×10^{16}	cm^{-3}

To account bandgap narrowing effects, BGN model was used. These effects may be described by an analytic expression relating the variation in bandgap,ΔE_g,to the doping concentration,N. The expression used in ATLAS is from Slotboom and de Graaf [13]:
The used values for the parameters BGN.E, BGN.N and BGN.C are shown in Table 2.3[13]:

Table 2.3: Default parameters of Slotbooms Bandgap Narrowing Model foe equation 2.11

Statement	Parameter	Default	Units
METERIAL	BGN.E	9.0×10^{16}	V
METERIAL	BGN.N	1.0×10^{16}	cm^{-3}
METERIAL	BGN.C	0.5	-

2.2 Simulation profile

Device simulation using silvaco atlas usually faces convergence problems and necessitates a long simulation run times. To avoid these problems, the simulation of silicon nanowire MOSFET has been divided into a few groups. At first, structure definition was performed. In this definition the simulation focused on creating the structure with a suitable mesh density. Regions and electrodes were defined as depicted in figure 2.2. Finer nodes were assigned in critical areas, such as across the gate oxide to monitor channel activity and to get a better picture of the depletion layer and junction behavior near the source/drain boundaries. A coarser mesh was used elsewhere in order to reduce simulation run time.

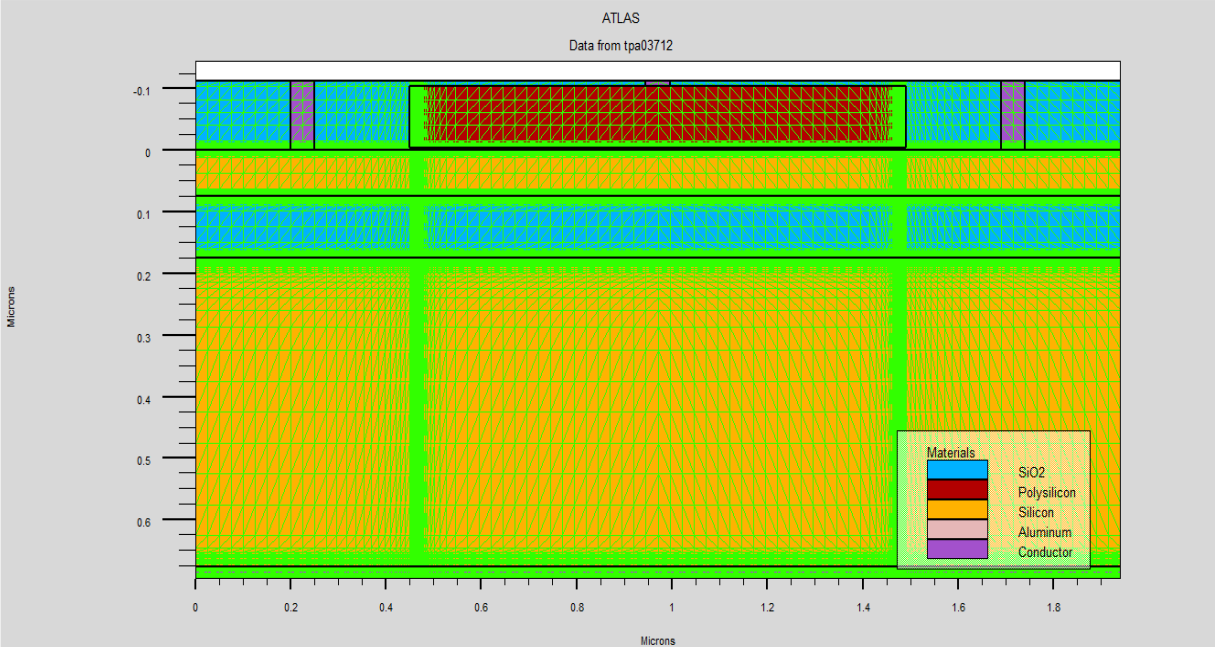

Figure 2.2: Cross-sectional view of p-type nanowire showing the mesh density used in this simulation.

Once the structure and the mesh were found to be as desired, the simulation was performed with appropriate models as discussed in section 2.1 and numerical solving methods. The model was invoked by using the statements FERMI, CVT, CONSRH, BGN. The numerical solving methods GUMMEL, NEWTON were used to reduce the simulation run time, while keeping the accuracy of the simulation at an acceptable level.

To get convergence, a special bias point solving method was used. It was found that the simulation faced difficulty in solving the initial desired bias points. i.e. ±1V, -2V, ±3V, ±4V, ±5V for backgate voltage and ±1V for drain voltage. Therefore, the initial gate bias was set to 0.005V and the next bias point was set to 0.05V, before finally setting the bias point to desired value.

CHAPTER 3: RESULTS

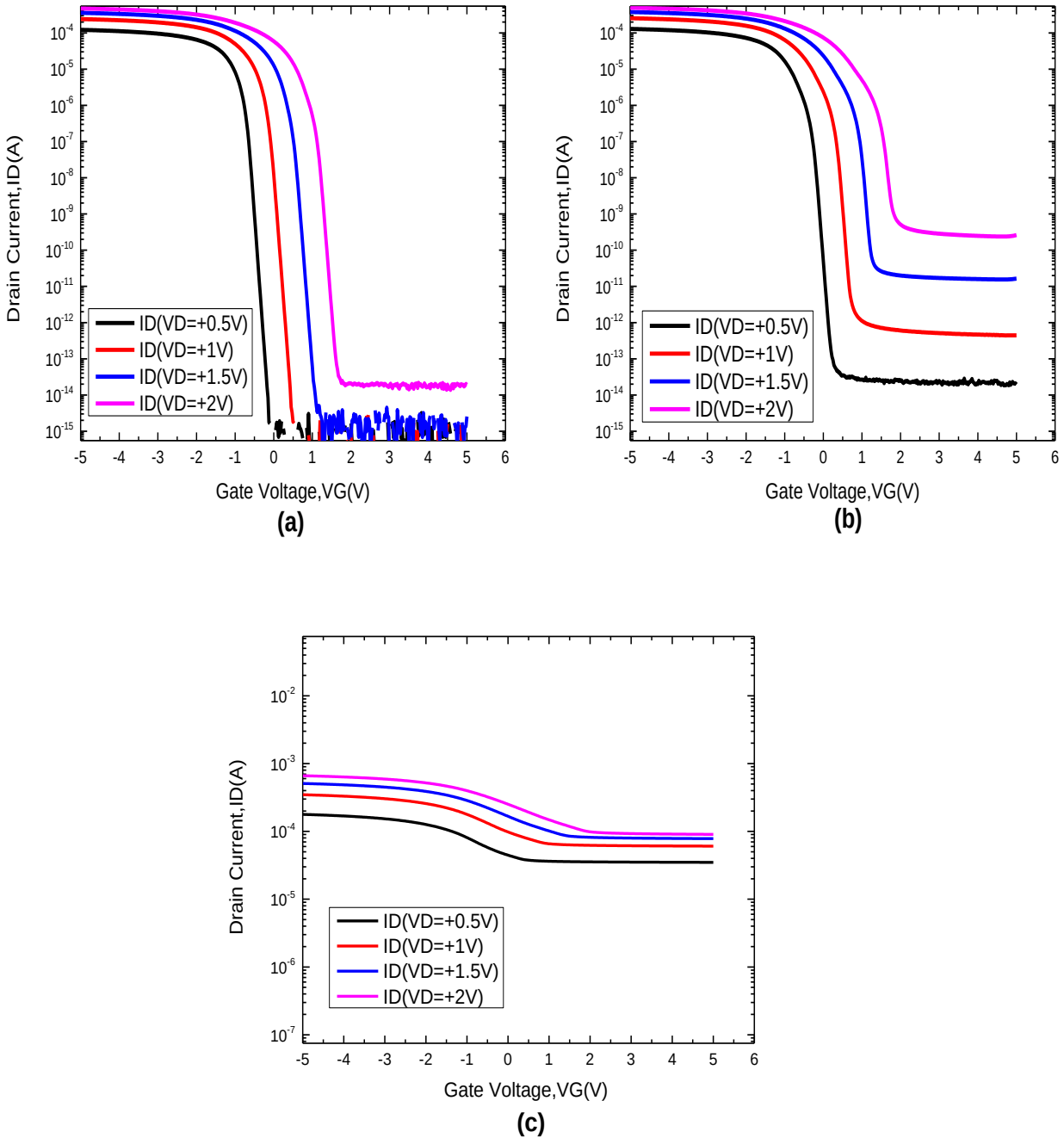

Figure 3.1: Transfer characteristics (I_{DS} Vs V_{GS}) of 75nm Si-NW when V_D is positive and V_G is swiped from +5V to -5V for $V_{Backgate}$= 0V for doping concentrations of a) $10^{16}cm^{-3}$ b) $10^{17}cm^{-3}$ and c) $10^{18}cm^{-3}$.

Figure 3.1 (a to c) shows transfer characteristics (I_D vs V_G) of Si-NW when V_D is positive and V_G is swiped from +5V to -5V and for backgate bias of 0V. The nanowire has thickness of 75nm for $10^{16}cm^{-3}$, $10^{17}cm^{-3}$and $10^{18}cm^{-3}$ doping respectively with channel length of 1µm. In fig 3.1 (a) for $10^{16}cm^{-3}$ doping sub-threshold slope is found to be 70.36mV/dec and DIBL 1100mV/V. This value of sub-threshold slope is promising for sensor. For $10^{17}cm^{-3}$ doping in fig 3.1 (b) the sub-threshold slopes is found to be 79mV/dec and DIBL 1200mV/V. The sub-threshold characteristic at this doping is inferior to $10^{16}cm^{-3}$. For $10^{18}cm^{-3}$ doping in fig 3.1 (c) the sub-threshold slope is found to be 3402.4mV/dec and DIBL 2660mV/V, implies that sub-threshold characteristics at $10^{18}cm^{-3}$ is severely degraded and hence it can be concluded that 75nm thick p-type Si NW can be applied as sensor for body doping of $10^{16}cm^{-3}$ and $10^{17}cm^{-3}$ but at $10^{18}cm^{-3}$ doping it will not exhibit viable sensor operation.

Figure 3.2 (a to c) shows transfer characteristics (I_D vs V_G) of Si-NW when V_D is positive and V_G is swiped from +5V to -5V and for backgate bias of 0V. The nanowire has thickness of 50 nm for $10^{16}cm^{-3}$, $10^{17}cm^{-3}$and $10^{18}cm^{-3}$ doping respectively with channel length of 1µm. In fig 3.2 (a) for $10^{16}cm^{-3}$ doping sub-threshold slope is found to be 68.34mV/dec and DIBL 1050mV/V which is actually good characteristics for using as biosensor. For $10^{17}cm^{-3}$ doping in fig 3.2 (b) the sub-threshold slopes is found to be 70mV/dec and DIBL 1100mV/V. This characteristic is comparably better than 75nm thick NW at this body doping concentration and hence, 50nm thick NW at $10^{17}cm^{-3}$ doping is also promising for sensor operation. For $10^{18}cm^{-3}$ doping in fig 3.2 (c) the sub-threshold slopes is found to be 2265.5mV/dec and DIBL 1900mV/V. Although these values are better than sub-threshold characteristics at this body doping for 75nm thick NW it is not suitable for using as sensor.

Figure 3.3 (a to c) shows transfer characteristics (I_D vs V_G) of Si-NW when V_D is positive and V_G is swiped from +5V to -5V and for backgate bias of 0V. The nanowire has thickness of 25nm for $10^{16}cm^{-3}$, $10^{17}cm^{-3}$and $10^{18}cm^{-3}$ doping respectively with channel length of 1µm. In fig 3.3 (a) for $10^{16}cm^{-3}$ doping sub-threshold slope is found to be 64mV/dec and DIBL 1050mV/V. The sub-threshold characteristics of 25nm thick NW is similar to 75nm and 50nm (Fig 3.1 and Fig 3.2) NWs at this doping and obviously ok for sensor design. For $10^{17}cm^{-3}$ doping in fig 3.3 (b) the sub-threshold slopes is found to be 65.49mV/dec and DIBL 1050mV/V. This value is much better than 75nm and 50nm thick NWs at this doping concentration and almost near to theoretical value of 60mV/dec. For $10^{18}cm^{-3}$ doping in fig 3.3 (c) sub-threshold characteristics is completely changed. 25nm thick NW at $10^{18}cm^{-3}$ doping exhibits much better sub-threshold behavior in comparison to 75nm and 50nm NWs with body doping of $10^{18}cm^{-3}$ thus the sub-threshold slope of 25nm is found to be 66.96mV/dec and DIBL 1100mV/V at $10^{18}cm^{-3}$ doping which is obviously promising as sensors.

To investigate the possibility of tuning NW's degraded sub-threshold characteristics backgate bias arrangement figure 3.4 (a to c) shows transfer characteristics (I_D vs V_G) of Si-NW when V_D is positive and V_G is swiped from +5V to -5V and for different backgate biases. These transfer characteristics are shown for nanowires having thicknesses of 75nm, 50nm and 25nm with

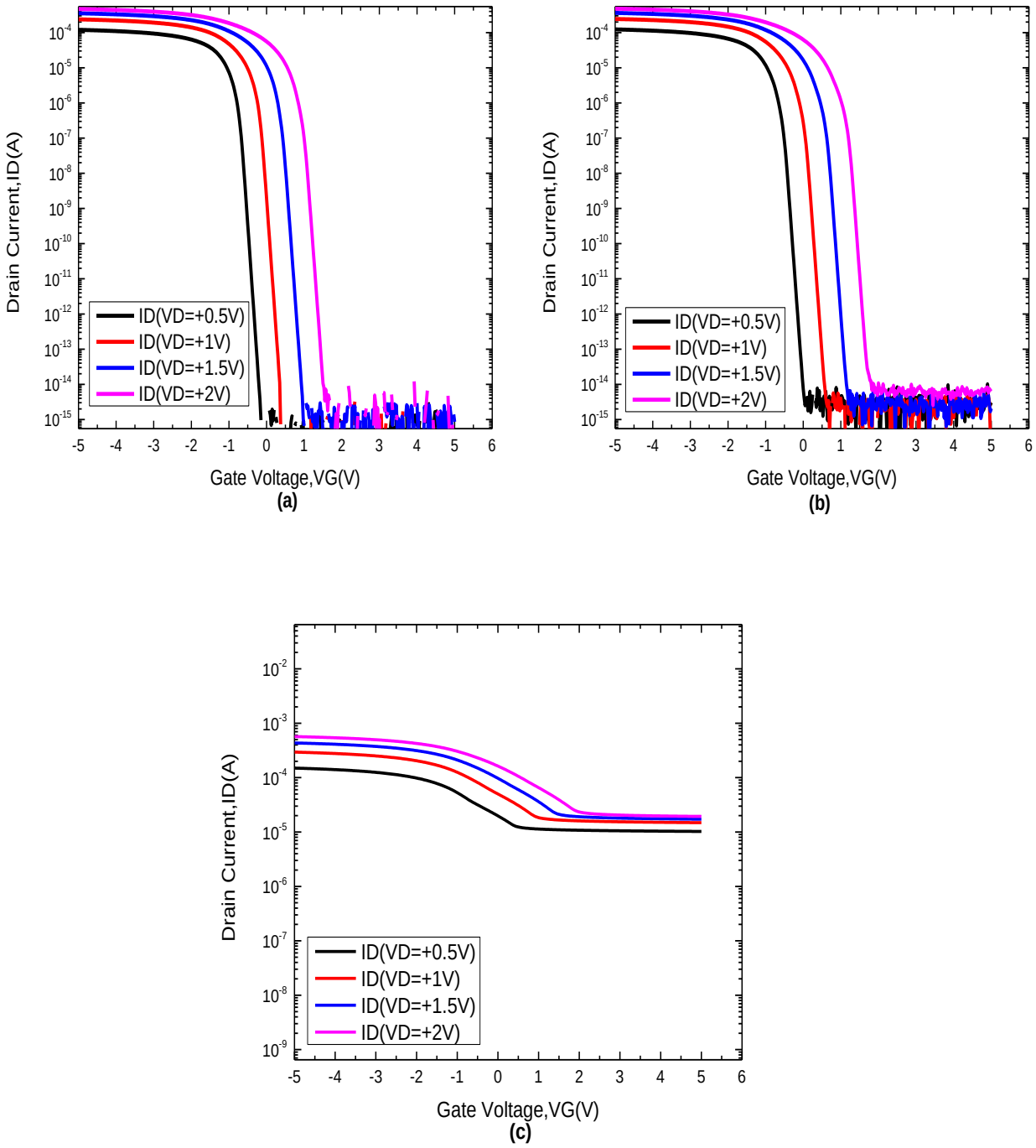

Figure 3.2: Transfer characteristics (I_{DS} Vs V_{GS}) of 50nm Si-NW when V_D is positive and V_G is swiped from +5V to -5V for $V_{Backgate}$= 0V for doping concentrations of a) $10^{16}cm^{-3}$ b) $10^{17}cm^{-3}$ and c) $10^{18}cm^{-3}$.

doping concentration of $10^{18}cm^{-3}$, a channel length of 1µm. During this simulation the drain voltage was positive and fixed at V_{DS}=0.5V while different backgate bias was applied. For 75nm Si NW at $10^{18}cm^{-3}$ doping in fig 3.4 (a) backgate voltage is not able to change NW's sub-threshold characteristics too much. While without any backgate voltage (0V) sub-threshold slope was 3402.4mV/dec. It is found to be 3983mV/dec for -7V of backgate voltage and 2756.7mV/dec for +7V of backgate voltage. In general it is observed that application of negative backgate voltage is degrading 75nm thick p-type Si NW's sub-threshold characteristics whereas application of positive backgate voltage is improving sub-threshold behavior.

For 50nm thick NW in fig 3.4 (b), sub-threshold characteristics are better than 75nm NW with a sub-threshold slope of 2265.6mV/dec when backgate bias was 0V. This value improves to 926.93mV/dec for +7V of backgate voltage whereas for -7V of backgate voltage it degrades to 2851.5mV/dec. This result shows that influence of backgate voltage on 50nm thick NW is higher than 75nm thick NW and hence sub-threshold slope change upon application of backgate voltage is high in 50nm NW. Although sub-threshold slope of 50nm NW is better than 75nm, 50nm NW still could not be used as good sensor. For 25nm thick Si NW in fig 3.4 (c) sub-threshold slopes is excellent with a value of 66.96mV/dec at 0V of backgate bias. This value merely improves to a value of 63.12mV/dec at +7V of backgate bias. Such a minor improvement with positive backgate bias at 25nm NW thickness implies that this is the best sub-threshold slope value that could be expected for $10^{18}cm^{-3}$ doping and for 25nm thick NW. However degradation of NW behavior is possible with application of negative backgate bias as can be seen from fig 3.4 (c). At -7V of backgate bias sub-threshold slope becomes 1517.1mV/dec. The result imply that among three thicknesses of NWs considered in this work 25nm thick NW would be the best platform for sensor at $10^{18}cm^{-3}$ doping with good backgate voltage.

Figure 3.5 (a to c) shows transfer characteristics (I_D vs V_G) of Si-NW at different backgate biases for body doping concentrations of $10^{17}cm^{-3}$ doping and for three different NW thicknesses. For NW thicknesses of 75nm in fig 3.5 (a), NW exhibit a sub-threshold slope of 79mV/dec when backgate voltage is 0V. Negative backgate voltage is found to degrade NW characteristics and at backgate voltage of -7V sub-threshold slope is 1850mV/dec. However positive backgate voltage is found to make minor improvement of sub-threshold slope. At +7V of backgate voltage slope improves to a value of 63mV/dec. This result imply that 63mV/dec sub-threshold slope is limited value for 75nm thick NW and no further improvement is possible by backgate. Almost similar characteristics are found for 50nm thick NW at $10^{17}cm^{-3}$ doping as shown in fig 3.5 (b). Sub-threshold slope values at 0V, +7V and -7V are found to be 70mV/dec, 61mV/dec and 1223mV/dec respectively implying that at body doping of $10^{17}cm^{-3}$, 75nm and 50nm thick NWs would exhibit similar sensor behavior. For 25nm thick NW (Fig 3.5-c) a drastic change in device characteristics is found. At backgate voltage of 0V, 25nm thick NW exhibit sub-threshold slope of 65.49mV/dec. In this thickness change in the sub-threshold slope upon application of backgate voltage is found to be lower in comparison to 75nm and 50nm NW for doping concentration of

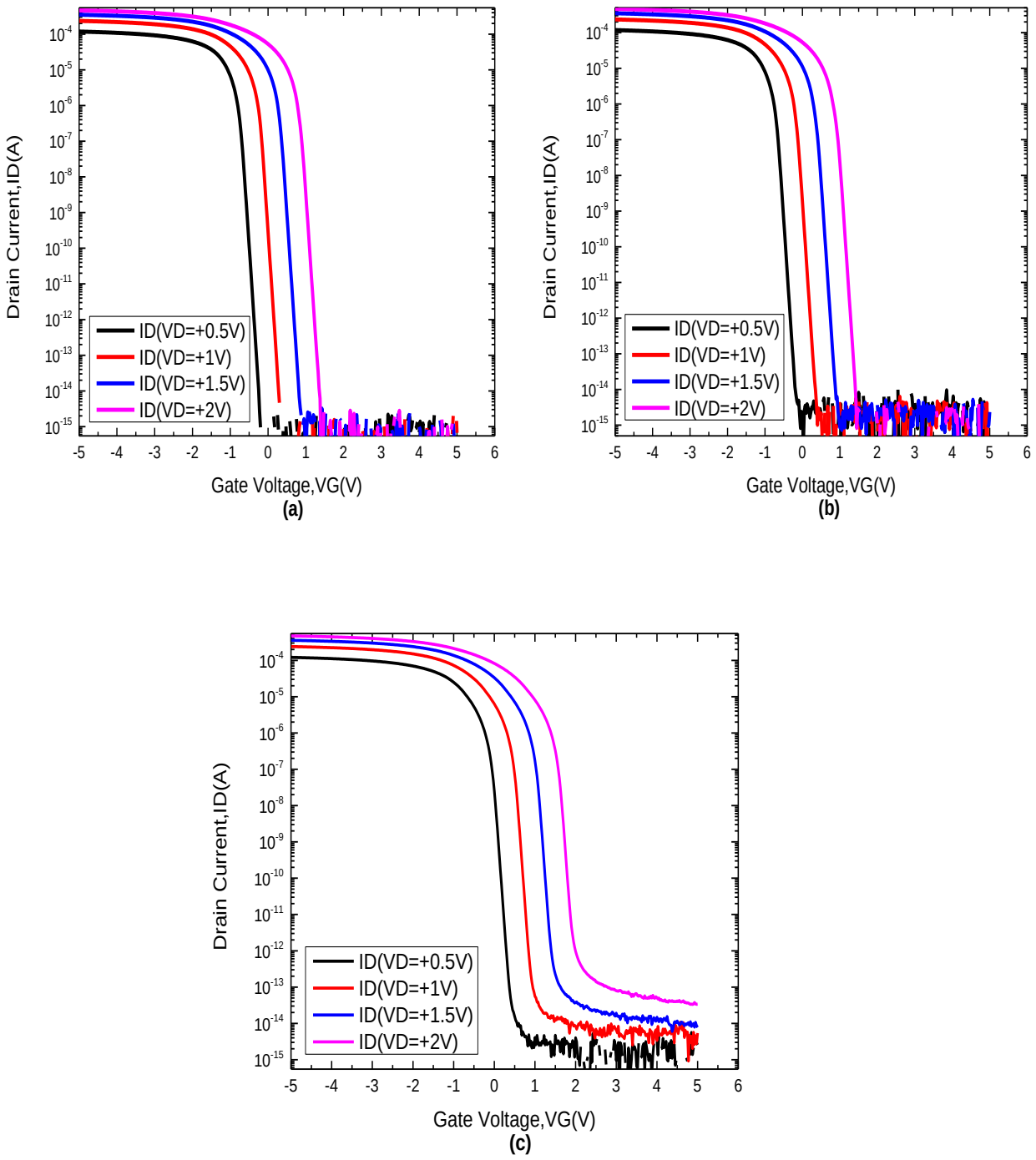

Figure 3.3: Shows transfer characteristics (I_{DS} Vs V_{GS}) of 25nm Si-NW when V_D is positive and V_G is swiped from +5V to -5V for $V_{Backgate}$= 0V for doping concentrations of a) $10^{16}cm^{-3}$ b) 10^{17} cm^{-3} and c) $10^{18}cm^{-3}$.

$10^{17}cm^{-3}$. NW's sub-threshold behavior remains immune to backgate bias at 25nm NW thickness for doping concentration of $10^{17}cm^{-3}$.

In Figure 3.6 (a to c) shows transfer characteristics (I_D vs V_G) of Si-NW when V_D is positive and V_G is swiped from +5V to -5V and for different backgate biases. We got these transfer characteristics for nanowires having thickness of 75nm, 50nm and 25nm with doping concentration of $10^{16}cm^{-3}$ with channel length of 1µm.

In general NW's sub-threshold behavior for body doping of $10^{16}cm^{-3}$ is similar to $10^{17}cm^{-3}$ doping at all thicknesses and hence it can be concluded that p-type Si NW's sensor behavior would be similar for body doping of $10^{16}cm^{-3}$ and $10^{17}cm^{-3}$.

Fig 3.7 shows extracted values of sub-threshold slopes as a function of backgate voltages for three body doping concentrations and for three thicknesses of Si NW. For NW thickness of 75nm in fig 3.7 (a) if can be seen that $10^{18}cm^{-3}$ NW's sub-threshold slope can be changed from 3983 mV/dec to 2756.7mV/dec while backgate voltage is varied from -7V to +7V. This value of sub-threshold slope is not suitable for sensor operation. For doping of $10^{17}cm^{-3}$ NW's sub-threshold slope is 79mV/dec at 0V of backgate voltage which degrades to a value of 1850mV/dec at -7V of backgate bias. However, application of positive backgate bias found to have minor effect on the sub-threshold characteristics with an exhibited value of 63mV/dec at backgate 7V. Almost similar behavior is observed for 75nm thick Si NW at a doping of $10^{16}cm^{-3}$. This result implies that for 75nm thick NW $10^{16}cm^{-3}$ or $10^{17}cm^{-3}$ concentrations can be chosen for sensor design.

An almost similar trend with body doping is also found for 50nm NW thickness. For 50nm NW again body doping $10^{18}cm^{-3}$ is not useable for sensor design and sub-threshold slope varies from 2851.5mV/dec to 926.9308mV/dec while backgate bias is varied from -7V to +7V. For body doping of $10^{17}cm^{-3}$ and $10^{16}cm^{-3}$ 50nm thick NW shows similar characteristics for 0V to +7V of backgate biases with sub-threshold slope value around 62mV/dec implying that at 50nm thickness both $10^{16}cm^{-3}$ and $10^{17}cm^{-3}$ doping can be used in NW sensor.

For 25nm thickness in Fig 3.7 (c) NW's sub-threshold behavior is degraded when negative backgate bias is applied. However from 0V to +7V of backgate biases 25nm thick Si NW shows similar sub-threshold slopes with values around 63mV/dec which is close to theoretically ideal sub-threshold slope of 60mV/dec. As a result it can be decided that 25nm thick Si NW can be designed using both low and high doping while doping is varied from $10^{16}cm^{-3}$ to $10^{18}cm^{-3}$.

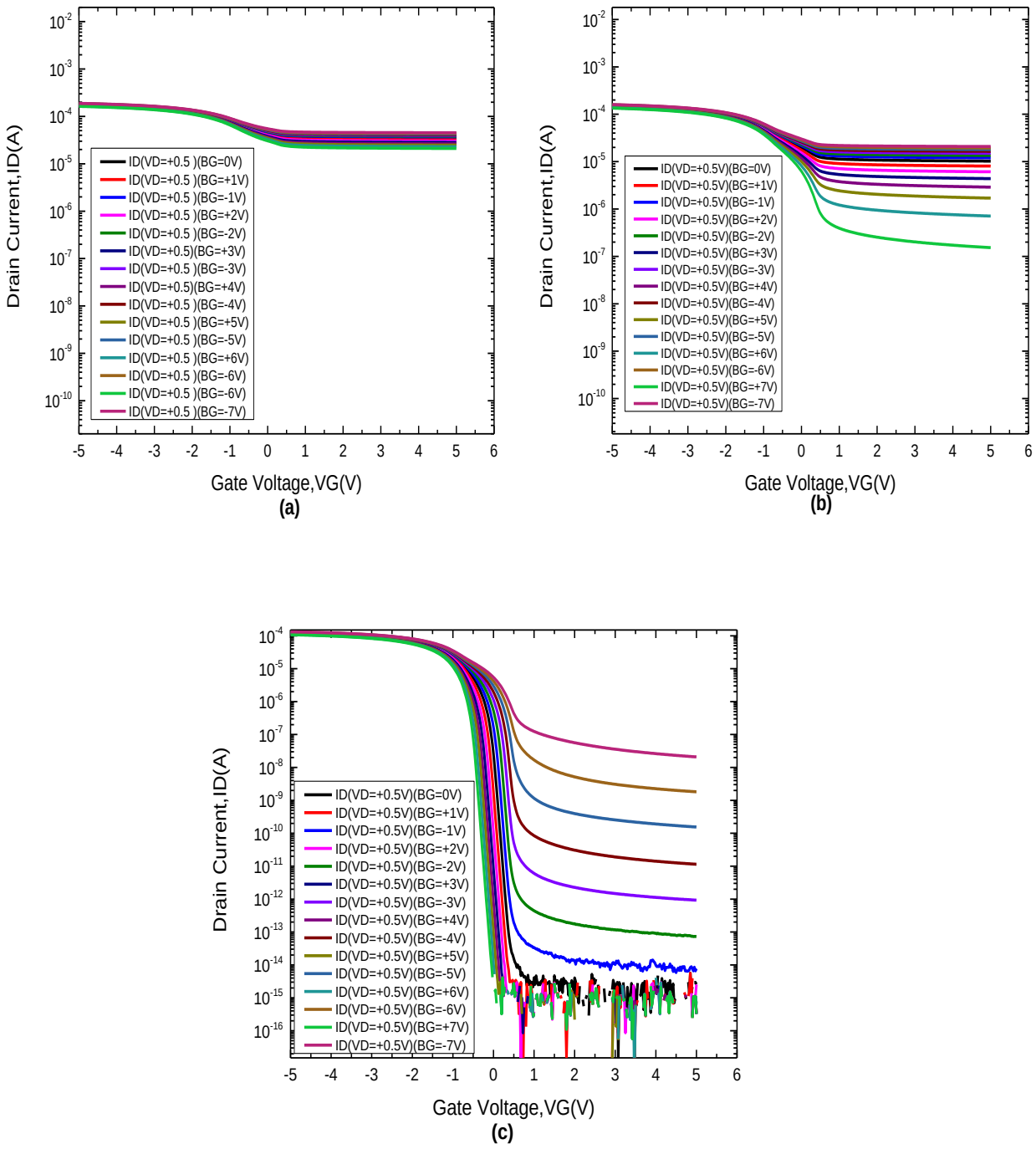

Figure 3.4: Shows transfer characteristics (I_{DS} Vs V_{GS}) of Si-NW having doping concentration of $10^{18}cm^{-3}$ when V_D is positive and V_G is swiped from +5V to -5V at different backgate biases for thicknesses a) 75nm b) 50nm and c) 25nm.

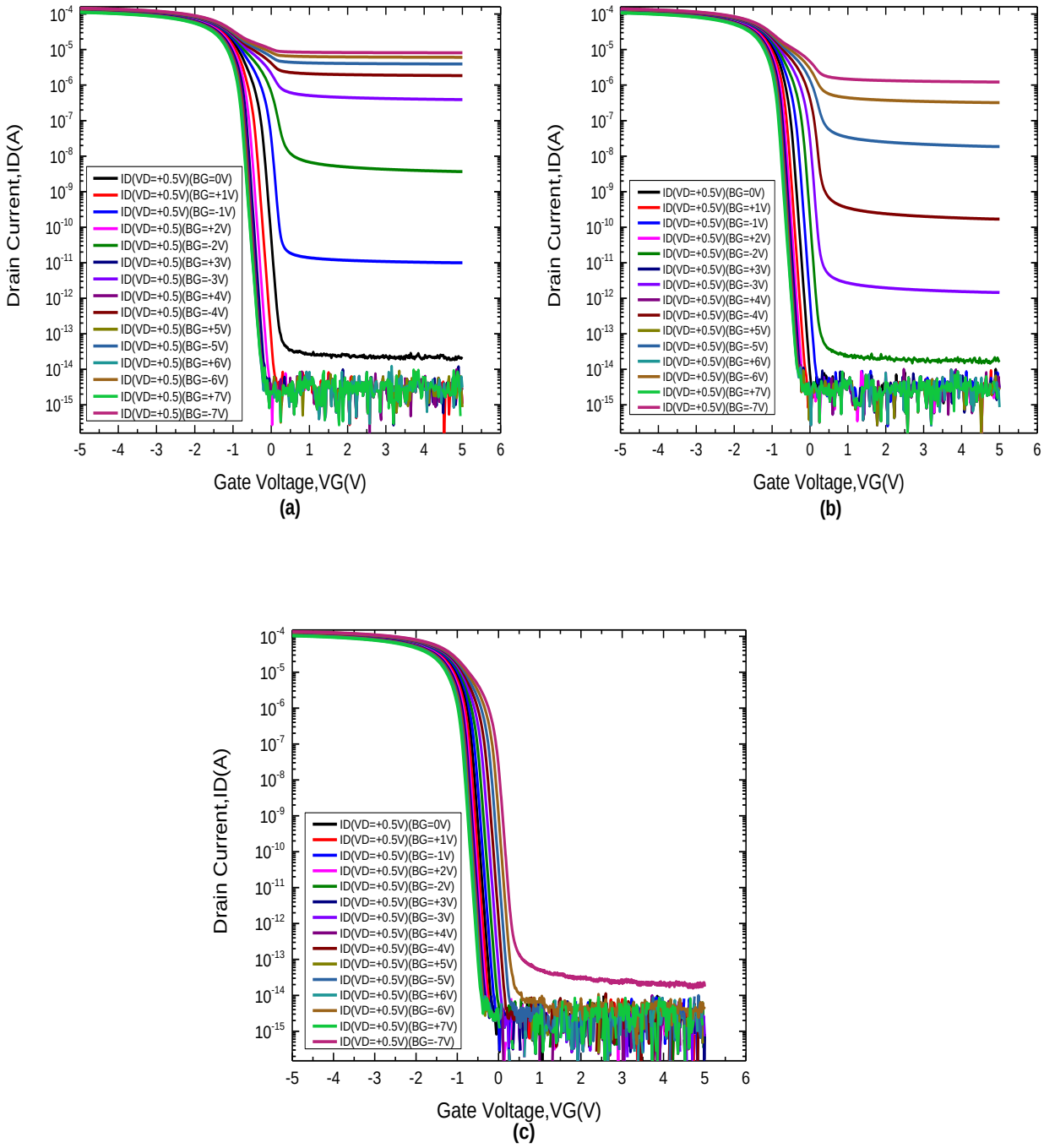

Figure 3.5: Shows transfer characteristics (I_{DS} Vs V_{GS}) of Si-NW having doping concentration of $10^{17}cm^{-3}$ when V_D is positive and V_G is swiped from +5V to -5V at different backgate biases for thicknesses a) 75nm b) 50nm and c) 25nm.

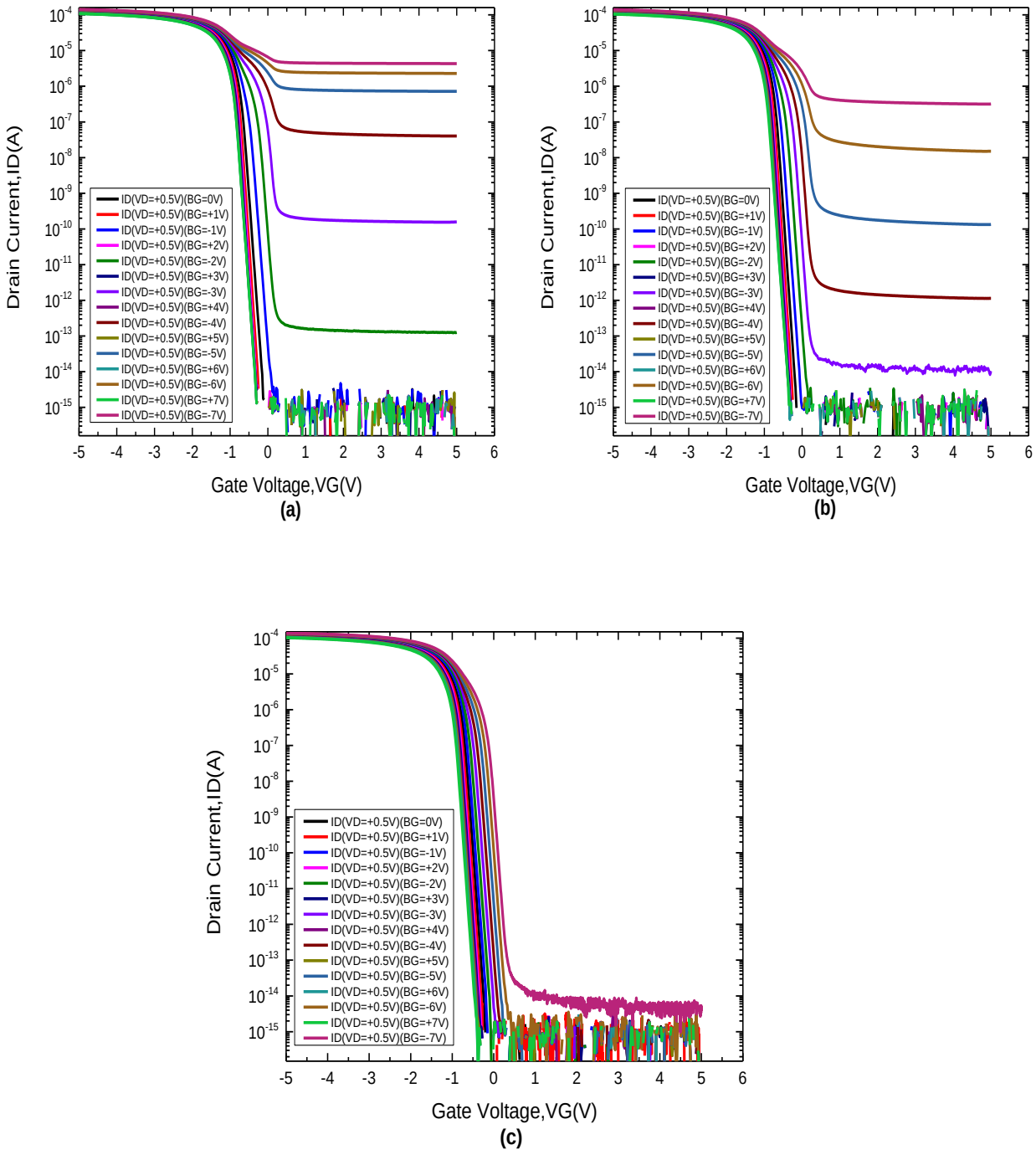

Figure 3.6: Shows transfer characteristics (I_{DS} Vs V_{GS}) of Si-NW having doping concentration of 10^{16} cm^{-3} when V_D is positive and V_G is swiped from +5V to -5V at different backgate biases for thicknesses a) 75nm b) 50nm and c) 25nm.

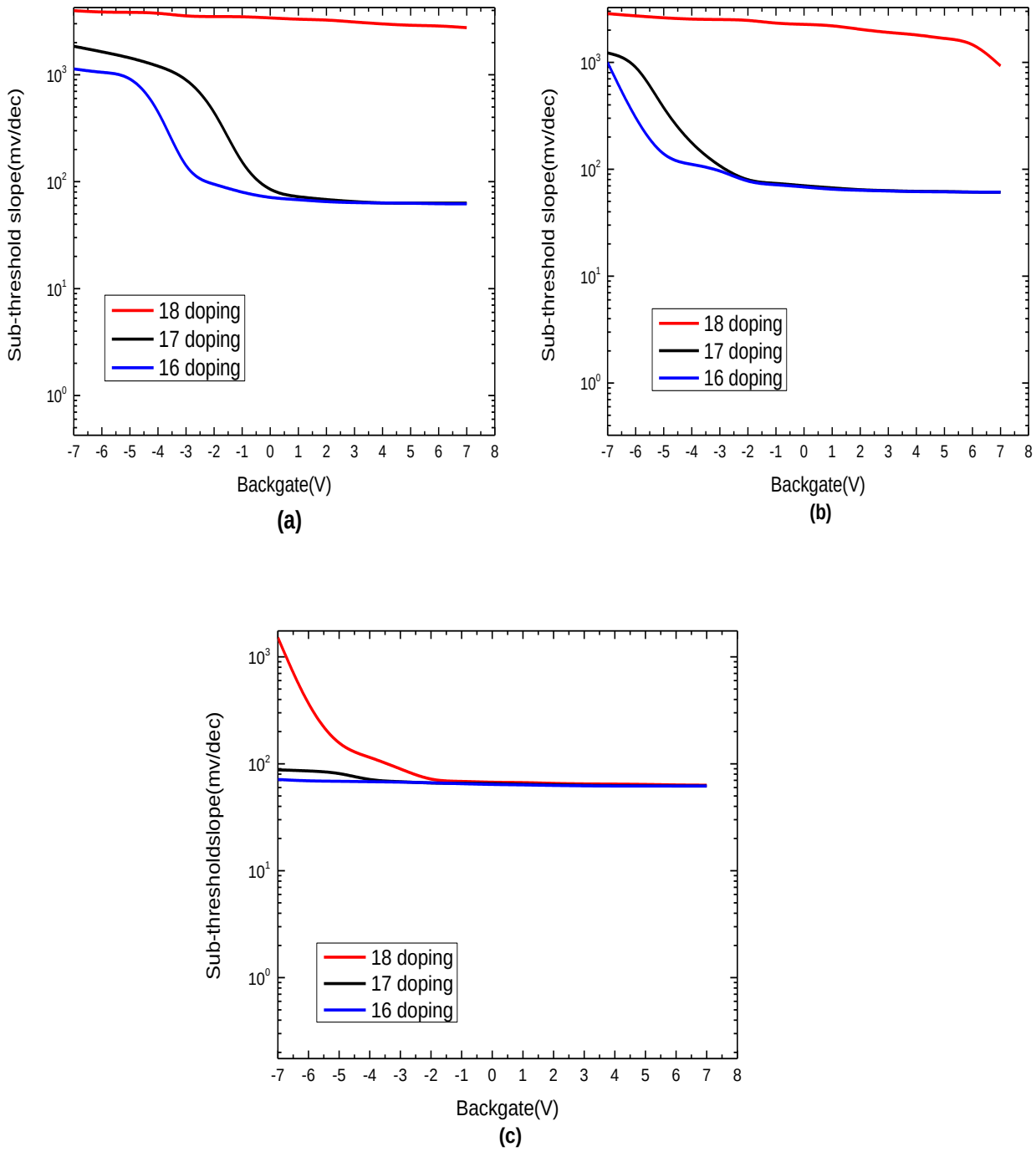

Figure 3.7: Shows sub-threshold slopes of Si-NW as a function of backgate voltages having doping concentrations of $10^{16}cm^{-3}$, $10^{17}cm^{-3}$ and $10^{18}cm^{-3}$ distinctly when V_D is positive for thicknesses a) 75nm b) 50nm and c) 25nm.

CHAPTER 4: DISCUSSION AND CONCLUSION

The aforementioned results show that Si NW behavior can be readily tailored using backgate bias arrangements. Generally p-type NW's characteristics show degraded behavior upon application of negative backgate voltages. This degradation can be explained by hole accumulation due to negative backgate voltage in the body of NW. For positive backgate voltage strong depletion in p-type Si makes effective doping thereby improves sub-threshold characteristics of NW. Effect of various backgate voltages on different thicknesses of p-type Si NW has been investigated. Backgate bias obviously showed significant change in device characteristics. 75nm thick NW shows sub-threshold slope of 70.36mV/dec, 79mV/dec and 3402.2mV/dec at doping values of $10^{16}cm^{-3}$, $10^{17}cm^{-3}$ and 10^{18} cm^{-3} respectively. This result shows that 75nm thick Si NW's sensor characteristics degrade with the increase of body doping values. Application of positive backgate has been found to improve NW's sub-threshold characteristics however this improvement is minor for 75 nm thick Si NW at $10^{18}cm^{-3}$ doping. This 25nm thick Si NW exhibited sub-threshold slopes of 64mV/dec, 65.49mV/dec and 66.96mV/dec at doping values of $10^{16}cm^{-3}$, $10^{17}cm^{-3}$ and $10^{18}cm^{-3}$ respectively which implies much better sensor operation of 25nm thick NW in comparison to 75 nm thick NW. Application of +7V of positive backgate bias resulted in the improvement of the sub-threshold slope of the 25 nm thick NW with values of 62mV/dec, 62mV/dec and 63.11mV/dec at doping values of $10^{16}cm^{-3}$, $10^{17}cm^{-3}$ and $10^{18}cm^{-3}$ respectively.

References:

[1] Y. Chen, X. Wang, M. K. Hong, S. Erramilli, P. Mohanty and C. Rosenberg," Nanoscale Field Effect Transistors for Biomolecular Signal Amplification", Appl. Phys., let. 91, pp. 243511, 2007.

[2] F. Patolsky, G. Zheng and C.M. Lieber, "Nanowire-Based Biosensors," Anal. Chern. 78, pp. 4260-4269, 2006.

[3] Cui, Y., and Lieber, C. M., "Nanowire and Nano sensor for highly sensitive and selective detection of biological and Chemical species", Science,vol.293,pp 1289-1292

[4] Y. Bunimovich, Y. Shin, W. Yeo, M. Amori, G. Kwong, and J. Heath, "Quantitative real time measurements of DNA hybridization with alkylated nanoxidized silicon nanowires in electrolyte solution," J. Am. Chern. Soc., vol. 128, pp. 16323-16331, Dec. 2006.

[5] Y. Wu, P. Hsu, and W. Liu, "Polysilicon wire for the detection of level free DNA," Journal of The Electrochemical Society, vol. 159, no. 6, pp.J191-J195, 2010.

[6] J. H. Chua, R.E. Chee, A. Agarwal, S.M. Wong, and G. Zhang, "Label-free electrical detection of cardiac biomarker with complementary metal-oxide semiconductor compatible silicon nanowire sensor arrays," Analytical Chemistry, vol. 81, no. 15, pp. 6266-6271, 2009.

[7] N.Elfstrom, A. Karstrom, and J. Linnors, "Silicon nanoribbons for electrical detection of biomolecules," Nano Letters, vol. 8, pp. 945-949, 2008.

[8] A. Cattani-Scholz, D.Pedone, M. Dubey, S. Peppi, S. Nickel, P. Feulner, J. Schwartz, G. Abstrelter, and M. Tornow," Organophosphonate-based pnafunctionalization of silicon nanowires for level free DNA detection," ACS NANO, vol. 2, no. 8, pp. 1653-1660, 2008.

[9] Mohammad M. A.Hakim, M.Lombardini, K.Sun, F.Giustiniano, P.L.Roach, D.E. Davies, P.H.Howarth, M. R. R.de Planque, H. Morgan, P. Ashburn, "Thin film polycrystalline silicon nanowire biosensors," Nano Letters, vol. 12, Issue 4, pp. 1868-1872, 2012.

[10] P.Hsu, J. Lin, W. Hung, and A.cullis, "Ultra-sensitive polysilicon wire glucose sensornusing a 3-aminopropyltriethoxysilane and polydimethylsiloxne-treated hydrophobic fumed silica particle mixure as the sensing membrane," Sensors and Actuators B: Chemical, pp. 273-279, 2009.

[11] Songyue Chen, Johan G. Bomer, Wilfred G. van der Wiel, Edwin T. Carlin, and Albert van der Berg, "Top-Down Fabrication of Sub-30nm Monocrystalline Silicon Nanowires Using Conventional Microfabrication," American Chemical Society ^{ACS}NANO, vol. 3, no. 11, pp. 3487-3490, 2009.

[12] J. Colinge, C. Lee, A. Afzalian, A. Dehdashti, I. Yan, R. Ferain, P. Razavi, B. O'Neil, A. Blake, M. White, A. Kelleher, B. McCarthy, and R. Murphy, "Nanowire transistors without junctions", Nature Nanotechnology, vol. 5, pp. 225-229, 2010.

[13] Atlas user's Manual: Device Simulation Software, 2008.